ACS APPLIED MATERIALS & INTERFACES

www.acsami.org

Research Article

Microporous Polyethersulfone Membranes Grafted with Zwitterionic Polymer Brushes Showing Microfiltration Permeance and Ultrafiltration Bacteriophage Removal

Ji Qin, Eric Ziemann, Edo Bar-Zeev, Sharon E. Bone, Yuanzhe Liang, Meagan S. Mauter, Moshe Herzberg,* and Roy Bernstein*

Cite This: *ACS Appl. Mater. Interfaces* 2023, 15, 18343−18353

Read Online

ACCESS | Metrics & More | Article Recommendations | Supporting Information

ABSTRACT: Virus removal from water using microfiltration (MF) membranes is of great interest but remains challenging owing to the membranes' mean pore sizes typically being significantly larger than most viruses. We present microporous membranes grafted with polyzwitterionic brushes (*N*-dimethylammonium betaine) that combine bacteriophage removal in the range of ultrafiltration (UF) membranes with the permeance of MF membranes. Brush structures were grafted in two steps: free-radical polymerization followed by atom transfer radical polymerization (ATRP). Attenuated total reflection Fourier transform infrared (ATR−FTIR) and X-ray photoelectron (XPS) verified that grafting occurred at both sides of the membranes and that the grafting increased with increasing the zwitterion monomer concentration. The log reduction values (LRVs) of the pristine membrane increased from less than 0.5 LRV for T4 (∼100 nm) and NT1 (∼50 nm) bacteriophages to up to 4.5 LRV for the T4 and 3.1 LRV for the NT1 for the brush-grafted membranes with a permeance of about 1000 LMH/bar. The high permeance was attributed to a high-water fraction in the ultra-hydrophilic brush structure. The high measured LRVs of the brush-grafted membranes were attributed to enhanced bacteriophages exclusion from the membrane surface and entrapment of the ones that penetrated the pores due to the membranes' smaller mean pore-size and cross-section porosity than those of the pristine membrane, as seen by scanning electron microscopy (SEM) and measured using liquid−liquid porometry. Micro X-ray fluorescence (μ-XRF) spectrometry and nanoscale secondary ion mass spectrometry showed that 100 nm Si-coated gold nanospheres accumulated on the surface of the pristine membrane but not on the brush-coated membrane and that the nanospheres that penetrated the membranes were entrapped in the brush-grafted membrane but passed the pristine one. These results corroborate the LRVs obtained during filtration experiments and support the inference that the increased removal was due to a combined exclusion mechanism and entrapment. Overall, these microporous brush-grafted membranes show potential for use in advanced water treatment.

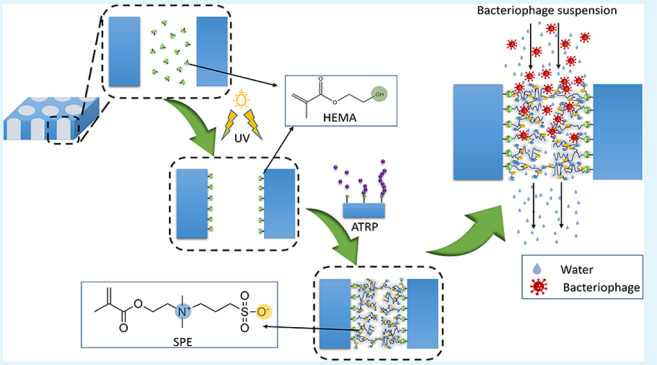

KEYWORDS: *microporous grafted membrane, SI-ATRP, polyzwitterion brush, virus removal, microfiltration*

1. INTRODUCTION

Waterborne pathogens, especially viruses such as adenovirus, enterovirus, hepatitis virus, norovirus, and rotavirus, are among the main water-related human health risks.[1] These viruses can cause outbreaks or sporadic cases of gastroenteritis, meningitis, respiratory disease, conjunctivitis, paralysis, hepatitis, or even death. Specifically, in developing countries where polluted water is often consumed, diarrheal diseases are the leading cause of child morbidity and mortality[2] and achieving at least a 4-log reduction for viral concentrations remains an important worldwide standard for water treatment processes.[3]

Viruses can enter drinking water through several pathways: through direct sewage discharge into water sources, either directly or when wastewater effluent is used for groundwater recharge;[4] through direct water reuse, a growing phenomenon in regions that face increased water demand, droughts, and anthropogenic pollution of other surface water supplies;[5] and through drinking water being elevated during severe flooding, and thus acquiring fecal pathogens from septic systems, which is a potential problem even in developed countries.[6]

Received: February 6, 2023
Accepted: March 16, 2023
Published: April 3, 2023

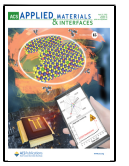

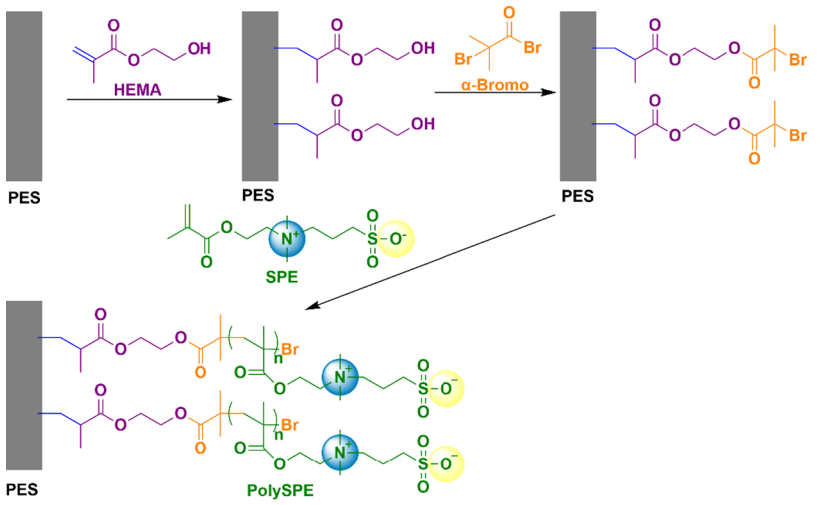

Figure 1. Schematic illustration of ATRP reaction of PES-polySPE brush membranes.

Most viruses transmitted by a fecal−oral route are highly persistent in water and can be found at high levels in treated water, even after decontamination processes commonly used for drinking water and wastewater.[7,8] For example, owing to their small size and unique surface properties, viruses are usually removed by coagulation, sedimentation, and granular media filtration by amounts typically less than the required by standards.[9−11] The inactivation of viruses can be improved by chemical disinfection, but this increases the risk of producing mutagenic and carcinogenic disinfection byproducts.[12] Ultraviolet and photocatalytic disinfection methods are not highly effective against viruses[13] or greatly depend on water quality.[14] Therefore, robust and cost-effective technologies for virus removal must be developed to purify various water resources.

Membrane filtration is a rapidly growing alternative technology for water purification requiring high viral removal.[15] It offers flexibility and versatility with a small footprint while producing high-quality water from a wide range of feedwater qualities. The membranes used for water treatment are typically porous pressure-driven microfiltration (MF) membranes with pore sizes of 0.1−10 μm and ultrafiltration (UF) membranes with pores of 2−100 nm. These membranes reject contaminants such as viruses by size exclusion. Therefore, MF membranes typically have limited viral removal (<0.5 log reduction value, LRV), although, as discussed below, some have demonstrated higher virus removal than expected based on size exclusion alone. In theory, UF membranes can almost completely remove most aquatic viruses (>6 LRV);[16,17] however, their removal rates can be lower than expected based on steric exclusion.[18] The downsides of UF membranes are increased energy demand and higher membrane surface area compared with MF membranes due to their significantly lower permeance.[19] An ideal membrane for treating water at low energy and low capital and operational costs would combine the flux of MF membranes with the viral removal potential of tight UF membranes.[20]

Various studies and membrane manufacturers have reported virus removal based on steric exclusion by MF membranes. High virus retention in these cases resulted from adsorption or physical entrapment.[15,21] Adsorption of viruses to the membrane surface or within its pores can be due to electrostatic[22] or hydrophobic[23] interactions that enhance the free energy of the system.[24] The virus adsorption capacity depends on the membrane material,[25] the type of virus (i.e., the capsid size and properties),[26,27] and solution properties.[28] Physical entrapment of viruses in the inner pore voids of the membrane is similar to the established removal mechanisms of particle entrapment inside depth filters.[29]

Recent research has demonstrated that virus retention by common MF and UF membranes could be increased by modifying the surface and pore structure, which primarily enhances adsorption interactions. For example, surface functionalization of a polyethersulfone (PES) membrane with polyethyleneimine (PEI) improved its removal of MS2 bacteriophages by about 3 LRV.[20] The removal rate increased to 5 LRV by optimizing the cross-linked PEI and incorporating antiviral nanoparticles.[30] Modifying electrospun nanofibrous MF membranes achieved 4 LRV for MS2 owing to elevated adsorption and smaller pores.[31] Some studies have suggested that in addition to reducing fouling,[32−34] zwitterionic modification can potentially increase membranes' ability to remove viruses from water.[35] Our previous work has demonstrated that a UF membrane modified using zwitterionic polymer increases MS2 and HAdV-2 removal by up to 4 LRV.[36] However, the permeate flux of the membrane was as low as ∼18 LMH/bar.

This study reports a new MF membrane that combines high bacteriophage removal and water permeance achieved through grafting zwitterionic polymer (polySPE) brushes to the microporous structure of a commercial PES MF membrane. The brushes were grafted using monomer solutions of different concentrations via free-radical polymerization followed by atom transfer radical polymerization (ATRP). Successful grafting throughout the membrane cross-section was verified by various methods. Membranes' virus removal potential was assessed using two bacteriophages (T4, ∼100 nm, and NT1, ∼50 nm). Surprisingly, although water permeance remained within the MF range, the LRVs for the bacteriophages were at the UF range. The high-water permeance was attributed to the super-hydrophilic polymer brushes containing a high-water fraction. The high removal of bacteriophages was ascribed to their entrapment in the microporous brush-grafted membrane. The suggested removal mechanism was supported by mass balance results measured during a T4 filtration cycle as well as micro-X-ray fluorescence (μ-XRF) mapping and nanoscale

https://doi.org/10.1021/acsami.3c01495
ACS Appl. Mater. Interfaces 2023, 15, 18343−18353

secondary ion mass spectrometry (NanoSims) with gold nanoparticles. Overall, the microporous polySPE brush-grafted MF membranes showed great potential for treating water to remove enteric viruses.

2. MATERIALS AND METHODS

2.1. Materials and Bacteriophages. Commercial PES MF membranes with a nominal pore size of 0.22 μm were obtained from TS Filter (Hangzhou, China). NaCl, 2-hydroxyethyl methacrylate (HEMA) (97%), and *N*-(3-sulfopropyl)-*N*-(methacryloxyethyl)-*N*,*N*-dimethylammonium betaine (SPE) were from Merck (Germany). Bacteriophage T4 (11303-B4TM) (~100 nm) and *Escherichia coli* host bacteria (11303TM) were from the American Type Culture Collection (Manassas, VA). Bacteriophage NT1 (~50 nm) and *Vibrio natriegens* host bacteria were from Laval University. Tryptic soy broth (TSB), ascorbic acid, copper(I) bromide (CuBr, purified, >99%), and 2,2-bipyridine (bipy) were from Sigma-Aldrich (Israel). 2-Hydroxy-4-(2-hydroxyethoxy)-2 methylpropiophenone (D2959) and α-bromoisobutyryl bromide (α-Bromo) were from Tokyo Chemical Industry (Japan). Copper(II) bromide ($CuBr_2$, purified, >99%) was from Acros Organics (Belgium). Methanol, ethanol, ethyl acetate, isopropanol (IPA), and diethyl ether (extra dry) were from BioLab (Israel) in AR grade.

2.2. Polymer Brush Grafting to the Microporous Membrane. Figure 1 (and Figure S1) shows the two-step ATRP approach to graft zwitterionic polymer (polySPE) brushes inside the MF membrane pores. First, HEMA was grafted into the PES pore walls by free-radical UV-irradiated grafting polymerization.[37,38] A PES coupon (44 mm diameter) was equilibrated in 50% IPA and then dried for 15 min under ambient conditions. The membrane was pre-wetted with ethyl acetate, placed in a beaker, and soaked in a 2×10^{-2} M solution of D2959 photoinitiator in ethyl acetate for 2 h in the dark. After draining the photoinitiator solution, the membrane was immersed for an additional 2 h in aqueous HEMA (150 mM); excess HEMA solution was then removed from the membrane surface using a scraper. Subsequently, the membrane was packed in a sealed plastic bag and clamped between two glass plates. The samples were irradiated under UV light (IntelliRay 400, Uvitron, USA) for 15 min with an irradiation intensity of 50 mW cm^{-2} covered with a glass filter to obtain hydroxyl groups grafted into the membrane pores (PES_OH). After grafting, each membrane was washed with 50% (v/v) ethanol/water for 24 h to remove unbound monomers and oligomers not covalently linked to the membrane walls. The modified membranes (PES_OH) were stored in ethanol until they were tested.

The polySPE brushes were grafted using SI-ATRP.[39] The ATRP initiator was then attached as a α-bromobutyryl ester to the PES_OH membranes. Membrane coupons were pre-dried for 15 min at ambient temperature and introduced into a pre-dried Schlenk flask (100 mL) under a nitrogen atmosphere charged with α-Bromo (1 mmol per coupon) in dehydrated diethyl ether (50 mL) cooled to −10 °C in an ice/acetone bath. Next, dry triethylamine (2.1 equiv total acyl halide) was gently introduced using a cannula. Aluminum foil wrapping protected the tube from light. After reaction for 1 h, when the coupling between the hydroxyl groups and ATRP initiator had been accomplished, the cooling bath was removed, and the reaction was continued with overnight stirring. The PES-α-Bromo ester coupon was retrieved, cleaned with water, and kept in a methanol and deionized water (4:1 v/v) solution until further use. In the last step, polySPE brushes were grafted into pores of the PES-α-Bromo ester membrane coupons by ATRP. Bipy (250 μmol; 39 mg per coupon), CuBr (100 μmol per coupon), and $CuBr_2$ (20 μmol per coupon) were added to a round-bottom flask. SPE monomer (5 mmol; 1.4 g) was in another Schlenk reaction tube. To avoid oxygen diffusion into the tubes, all reactors were previously degassed by three freeze−thaw cycles, and every subsequent step was conducted under continual N_2 flow. A mixture of methanol and deionized water (4:1 v/v) solution previously bubbled with nitrogen for 10 min was added to both tubes (5 mL to the flask containing the ligand and catalyst and 45 mL to the tube containing the monomer). The tubes were then left under stirring at 35 °C until complete dissolution of the SPE monomer. Subsequently, four initiator-coupled membrane coupons (PES-α-Bromo ester) were placed inside the Schlenk reaction tube containing the monomer. Then, 5 mL of CuBr/$CuBr_2$/Bipy solution was transferred to the Schlenk reaction using a nitrogen-purged syringe. Finally, 0.3 mL of ascorbic acid (0.02 M) was added dropwise to the reaction tube. The ATRP reaction took place for 4 h at 35 °C under continuous stirring. The grafted membranes (PES_0.1) were then taken from the polymerization solution, washed with water, and stored at 4 °C until further used. The PES_0.2 and PES_0.5 membranes were obtained using 0.2 and 0.5 M SPE, respectively (instead of 0.1 M SPE), under otherwise identical reaction conditions.

2.3. Membrane Characterization. A spectrometer (Vertex 70 FTIR, Bruker) equipped with a diamond/KRS-5 ATR crystal (Pike Technologies) recorded attenuated total reflection Fourier transform infrared (ATR−FTIR) spectra: 30 scans were taken at a resolution of 4 cm^{-1} for each spectrum. Both sides of a dry membrane (up and down) were measured. The degree of grafting (DG, eq 1) for each modified membrane was measured by ATR−FTIR spectroscopy:[40,41]

$$\mathrm{DG} = \frac{I_{\mathrm{mon}}}{I_{\mathrm{mem}}} \tag{1}$$

where I_{mon} is the intensity at 1040 cm^{-1}, representing a characteristic band of the grafted SPE polymer, and I_{mem} is the intensity at 1586 cm^{-1} for a band of the MF PES pristine membrane. The reported DG values are the average of at least three measurements on three distinct samples; the error bars represent the standard deviation. High-resolution X-ray photoelectron (XPS) spectra were collected using a spectrometer (ESCALAB-X, Thermo Scientific) with ultrahigh vacuum (1×10^{-9} bar) apparatus, an AlKα X-ray source, and a monochromator. The X-ray beam size was 500 μm. Survey spectra were recorded with a pass energy of 150 eV, and high-energy-resolution spectra were recorded with a pass energy of 20 eV. All spectra were calibrated relative to a carbon C 1s peak at 284.8 eV to correct for charging effects. The atomic ratios were calculated from the peak intensity ratios and the reported atomic sensitivity factors. Membranes' surface hydrophilicity was determined by measuring the contact angle of a sessile drop (20 μL) using an optical measurement system (OCA 15 plus, Data physics, Filderstadt, Germany). The reported values are the average of at least five measurements per sample for three distinct samples; the errors represent standard deviations. The mean pore diameter and pore-size distribution were determined by measuring liquid−liquid displacement using a liquid−liquid porometer (LLP). The membrane was pre-wetted with IPA as a wetting fluid, and the intrusion fluid was fluorated hydrocarbon with a surface tension of 15.9 dyn/cm. The pore-size distribution was calculated from the LLP isotherm data. Membranes' surface and cross-sectional morphology were ascertained by scanning electron microscopy (SEM, JSM-6010 L). The samples were dried at 40 °C in a vacuum oven overnight and sputtered with Au before introduction to the microscope. Cross-sectional imaging used membranes broken using liquid nitrogen.

Filtration experiments were conducted using a stirred dead-end cell (Amicon 8050, Millipore). The membranes were first compacted by filtering DI water at 0.2 bar until a constant flux was observed. Membrane permeability (L_p) was then calculated as follows:

$$L_p = \frac{V}{\Delta t \times A \times \Delta P} \tag{2}$$

where V (L) is the amount of collected water, Δt (h) is the duration, A (m^2) is the active surface area of the membrane, and ΔP (bar) is the transmembrane pressure (TMP). The reported value of L_p is the average of at least three measurements; the error represents standard deviation.

2.4. Propagation, Purification, and Quantification of T4 and NT1. *2.4.1. Host Culture Preparation.* The host bacteria inoculum was recovered and streaked onto a fresh TSB (for *E. coli*) or Luria−Bertani (LB) (for *V. natriegens*) plate from frozen glycerol stocks (stored at −80 °C) and incubated overnight at 37 °C for *E. coli* and at

https://doi.org/10.1021/acsami.3c01495
ACS Appl. Mater. Interfaces 2023, 15, 18343−18353

26 °C for *V. natriegens*. A single colony from a plate was inoculated into 20 mL of TSB or LB and incubated overnight at 37 or 26 °C. Experiments were conducted using at least two overnight cultures diluted once a day. An aliquot (100 μL) of the overnight cultured solution was cultivated into 25 mL of fresh TSB or LB and grown for 3 h to the exponential phase (having an optical density of 0.2−0.4 at 600 nm). Figure S3 gives the scheme of log-phase *E. coli* culture.

2.4.2. Bacteriophages Stock Propagation. Bacteriophages were unfrozen and propagated following Adams.[42] To initiate this process, the host bacteria (1 mL, log phase) were mixed with 100 μL bacteriophages and 5 mL of sterile, liquefied, soft agar (30 mg/mL TSB or LB + 0.5% agar), added to TSB or LB plates, and incubated overnight at room temperature. Sterilized phosphate-buffered saline (PBS) (10 mL) was then poured into the incubated bacteriophage plate, which was incubated at 37 or 26 °C for 1 h. The supernatant of PBS and bacteriophages was collected using a sterile pipette and then centrifuged (8000×*g*) for 15 min. The concentrated bacteriophages were filtered through a 0.45 μm filter and stored at 4 °C.

2.4.3. Overlay Technique for Bacteriophage Quantification. Bacteriophage titer was evaluated by preparing successive 10-fold bacteriophage dilutions, and the concentration of plaque-forming units (PFU) was determined using the double agar layer technique. Log-phase bacterial host (1 mL) and a suitable bacteriophage dilution (100 μL) were combined with 5 mL of molten soft agar, put onto a TSB solid medium plate that had previously been made, and solidified at room temperature. The sample was then incubated at 37 °C overnight. The plaques were counted, and the titer of the bacteriophages was evaluated in terms of PFU/mL:

$$\text{phage titer}\left(\frac{\text{PFU}}{\text{mL}}\right) = \frac{\text{average no. of plaques}}{\text{dilution} \times \text{volume of diluted virus}} \quad (3)$$

Positive controls (i.e., without added bacteriophages) and negative controls (i.e., without added bacteriophages or host bacteria) were made for all PFU tests. Figure S4 shows images of plaques formed by the two bacteriophages in both control tests.

2.5. Bacteriophage Suspension Filtration. Bacteriophage filtration tests were carried out using a dead-end filtration cell (Amicon 8050). Before each test, the background solution (NaCl, 10 mM) was passed through the membrane for 2 h until a stable flux was obtained. Bacteriophage filtration was then carried out with the modified and pristine membranes under the same initial permeate flux (≈200 LMH). The pressure (20−250 mbar) during filtration was monitored using a pressure gauge connected to the computer (Figure S2). The influent concentration of bacteriophage in this experiment was 10^4 to 10^5 PFU/mL. Permeate samples were collected intermittently during the filtration experiment, and the bacteriophage concentration in each sample was measured. The LRVs for bacteriophage were calculated as follows:

$$\text{LRVs} = -\log 10\left(\frac{C_p}{C_f}\right) \quad (4)$$

where C_f and C_p are the concentrations of the bacteriophage in the feed and permeate, respectively.

In addition, bacteriophage mass balance (for the pristine membrane and PES_0.1) was also found by evaluating the bacteriophage concentration trapped in the membrane. At the end of the filtration experiment, the membrane was flipped and backwashed with the background solution (50 mL), the solution was collected, and the bacteriophage concentration in the solution was measured. The membrane was then removed, a 1 cm^2 piece of it was placed in 10 mL of background solution and sonicated for 5 min in a sonication bath, and the phase concentration in the solution was measured.

2.6. μXRF Mapping of Si-Coated Gold Nanoparticles on the Membrane. 100 nm Si-coated gold nanospheres were filtered through the pristine and microporous brush-grafted MF PES membranes. The 10^7 nanoparticles/mL suspension of Si-coated gold nanospheres in 10 mM NaCl solution was filtered through these membranes at similar flux conditions as the bacteriophage suspension filtration tests (≈200 LMH) for 30 min. The samples underwent μ-XRF analysis without dehydration, maintaining the water content in the membrane pores. Two-dimensional μ-XRF maps were collected at beamline 2−3 at the Stanford Synchrotron Radiation Lightsource (SSRL) using a Si(111) double-crystal monochromator. Membranes were cut into 50-μm-thick sections using a Leica Cryotome. The sections were placed on a polycarbonate window and set in the path of the beam. Images of the membranes were collected at a step size of 1 or 5 μm. Fluorescence from Au and S was detected at 12,200 eV using a single-element Vortex Si-drift detector. Image analysis was conducted using SMAK.[43] A Pt fluorescence peak attributable to the beamline optics was detected. The Au and Pt fluorescence peaks overlap, leading to a background underneath the Au fluorescent peak. To account for this background, the energy dispersive spectrum for each pixel in the map was fit to quantify Au and Pt fluorescence intensity. The concentration of Au (μg/cm^2) was then calculated based on the Au fluorescence intensity using a reference foil of known concentration (47.6 μg/cm^2).

2.7. Depth Profiling of Si-Coated Gold Nanoparticles in the Membrane via NanoSIMS. High-resolution secondary ion maps were acquired for the pristine and brush-modified membranes used for μ-XRF mapping. Mapping employed a NanoSIMS 50 L ion microprobe (CAMECA, France) at the Stanford Nano Shared Facility, Stanford, CA, USA. Before analysis, membranes were dried at room temperature under vacuum and then coated with 10 nm carbon to prevent charging. A Cs^+ primary ion beam (current 15 pA, primary energy 8 keV, and extracting energy 8 keV) with a nominal spot size of 50 nm was used to raster over the area of interest. Seven distinct secondary ion species were detected ($^{12}C^-$, $^{14}N^-$, $^{16}O^-$, $^{28}Si^-$, $^{32}S^-$, $^{35}Cl^-$, and $^{197}Au^-$) using electron multipliers. Depth profiles of the seven species were acquired for both membranes.

2.8. Quantification of Bacteriophage Removal by the Modeling Transport Hindrance. The sieving coefficient with the hydrodynamic hindrance factors taken from Bungay and Brenner[44] was used to assess bacteriophage removal by size exclusion.[45] The T4 and NT1 bacteriophages are set to have diameters of 100 and 50 nm, respectively.[46,47] The sieving coefficient $S(r)$ was calculated as follows under an assumption of spherical particles in convective transport:[48]

$$S(r) = \frac{C_p}{C_f} = \begin{cases} 0 & \lambda \geq 1 \\ (1-\lambda)^2 \times [2-(1-\lambda)^2] \times \exp(-0.7146 \times \lambda^2) & \lambda < 1 \end{cases} \quad (5)$$

where λ is the ratio of the particle (bacteriophage) size (r_{phage}) and the average pore size (r):

$$\lambda = \frac{r_{phage}}{r} \quad (6)$$

To calculate the LRV for real membranes with polydispersed pore-size distributions, the particle retention must be considered across the entire membrane pore-size distribution. The overall LRVs are then calculated by integration to find the number of particles in the filtrate and the filtrate volume:[49,50]

$$\text{LRVs} = \log\left[\frac{\int_0^\infty f(r) \times dr}{\int_{r_{phage}}^\infty f(r) \times S(r) \times dr}\right] \quad (7)$$

where $f(r)$ is the pore-size distribution determined from LLP data using log-normal distribution fitting:[51]

$$f(r) = \frac{1}{r \times \sigma \times \sqrt{2\pi}} e^{-\ln(r/\mu)^2/2\sigma^2} \quad (8)$$

where μ is the mean pore size, and σ is the standard deviation.

2.9. Statistical Analysis. Statistical analyses (*t*-tests) to estimate the significance of differences between any two samples were performed using Origin software with $^*p < 0.05$ and $^{**}p < 0.01$.

https://doi.org/10.1021/acsami.3c01495
ACS Appl. Mater. Interfaces 2023, 15, 18343−18353

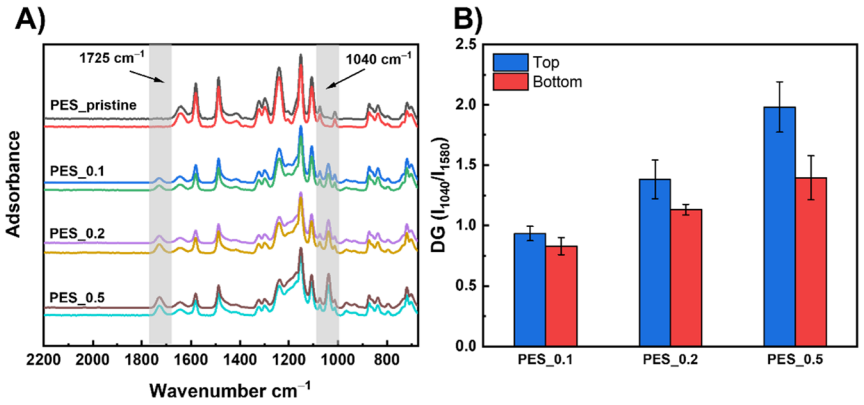

Figure 2. (A) ATR−FTIR spectra of PES_pristine, PES_0.1, PES_0.2, and PES_0.5, taken from the top and bottom sides. (B) DGs of the modified membranes are expressed as mean ± SD; n = 3.

Table 1. Elemental Composition (at %) Obtained by XPS for Both Sides (Top/Bottom) of the PES_pristine, PES_0.1, PES_0.2, and PES_0.5 Membranes

	%$C1_S$	%$N1_S$	%$O1_S$	%$S2_P$	C/N	C/O
	top/bottom				top/bottom	
PES_pristine	70.65/69.79	3.17/4.12	19.96/20.37	6.21/5.73	22.28/16.94	3.54/3.43
PES_0.1	64.34/64.83	5.17/4.58	24.49/24.77	6.01/5.82	12.44/14.16	2.63/2.62
PES_0.2	64.11/63.89	4.89/4.58	27.29/26.57	3.71/4.96	13.11/13.95	2.35/2.4
PES_0.5	64.69/65.41	5.52/4.91	25.24/24.14	4.55/5.55	11.72/13.32	2.56/2.71

3. RESULTS AND DISCUSSION

3.1. Membrane and Surface Characterization. Figure 2A presents ATR−FTIR spectra of pristine and microporous brush-grafted membranes at the three SPE concentrations (PES_0.1, PES_0.2, and PES_0.5). Modification with polySPE led to two new peaks at 1045 and 1725 cm^{-1} in all spectra. These peaks are assigned respectively to the sulfonic and carbonyl groups of the polySPE. Their similar intensities on both sides of the modified membranes suggest that polySPE successfully grafted through the membrane pores. In addition, the DG of the modified membranes (Figure 2B) gradually increases with SPE concentration and is slightly higher on the top than on the bottom side of the microporous brush-grafted membranes, with the difference increasing with increasing monomer concentration. Nevertheless, these differences are relatively minor and support the assumption that the micropores were successfully grafted with polySPE.

The XPS results in Tables 1 and S1 further confirm the successful grafting. The C/N and C/O ratios decreased following modification owing to higher N and O fractions and lower C fractions in the polySPE relative to those in the pristine PES membrane. In addition, both sides of each membrane showed similar atomic compositions, indicating modification of the entire cross-section. The pristine sample contained N, probably because of additives in the commercial PES membrane. The HR-XPS spectra (Table S1) reveal that the N 1s peak of the pristine PES comprises two peaks: a major peak at 399.5 eV and a minor peak at 402 eV. The major peak can be attributed to polyvinylpyrrolidone additive. The minor, a quaternary amine peak, was also due to additives in the pristine membrane.[52] The ratio between the N1 peak at 402.1 eV and the peak at 399 eV significantly increased following modification owing to an increased fraction of the quaternary ammonium groups from SPE. In addition, the HR-XPS (Table S1) found a new peak at 288.6 eV associated with the carbonyl groups (O−C═O) of HEMA or SPE, which appeared after the grafting of polySPE.

Contact angles of the pristine and microporous brush-grafted PES membranes were also measured. Figure 3 shows

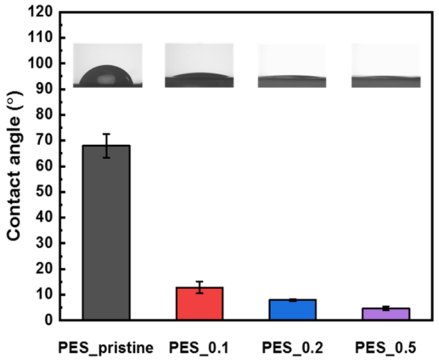

Figure 3. Contact angles of PES_pristine, PES_0.1, PES_0.2, and PES_0.5 expressed as mean ± SD; n = 5.

the decreasing contact angles of the membranes with their increasing PES content: from 68° ± 5° for the pristine membrane to 13° ± 2°, 8° ± 1°, and 5° ± 1° for grafted membranes PES_0.1, PES_0.2, and PES_0.5, respectively. This was most likely due to the increasing trend in DG (Figure 2B) and the associated higher hydration of the grafted zwitterionic polymer.[53]

The average pore size and the PDS were calculated using LLP and fitting the results to a log-normal probability distribution using eq 8. Figure 4A shows the average pore size of the PES_pristine membrane to be ≈300 nm. The mean size decreased and the distribution narrowed following grafting, with these changes becoming greater as the SPE monomer concentration increased, as has been found by others,[54,55] especially when ATRP was applied.[56] As the

https://doi.org/10.1021/acsami.3c01495
ACS Appl. Mater. Interfaces 2023, 15, 18343−18353

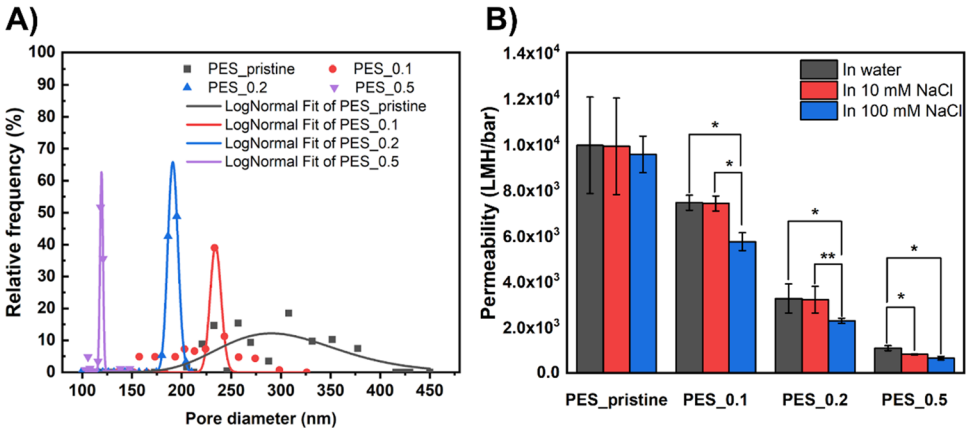

Figure 4. (A) Log-normal fits of the pore-size distributions of pristine and microporous brush-grafted PES at the three SPE monomer concentrations calculated based on liquid−liquid porometry measurements. (B) Water and salt solution (10 and 100 mM NaCl) permeability of the membranes expressed as mean ± SD (n = 3) and analyzed by t-testing: *p < 0.05, **p < 0.01.

wetting fluid used for the LLP measurements was IPA, a non-solvent for SPE,[57] the mean pore size in aqueous solutions is expected to be smaller due to brush swelling.[58−60]

Figure 4B displays the pure water (DI water) permeance (L_p) and permeate flux of salt solution (10 and 100 mM NaCl, measured at TMP = 0.1 bar) for the pristine and microporous brush-grafted membranes. As expected, the permeance of the PES_0.1 membrane (7456 LMH/bar) was lower than that of the pristine PES membrane (9967 LMH/bar). Permeance further decreased (to 3260 LMH/bar for PES_0.2 and 1088 LMH/bar for PES_0.5) as the SPE monomer concentration increased. However, as polySPE is salt-responsive, the membranes' permeate flux was also estimated using salt solutions. An insignificant decrease (<5%) in the permeate flux occurred when using salt solution compared with pure water (under similar TMP) with PES_pristine. Although similar permeate fluxes were recorded for PES_0.1 and PES_0.2 with pure water and low ionic strength solution (10 mM NaCl), the permeate fluxes of these membranes using 100 mM NaCl were, respectively, 9 and 24% lower than those using pure water (p < 0.05). PES_brush_0.5 showed an even greater reduction: a 25% decrease in permeability using 10 mM NaCl and a 45% decrease with 100 mM NaCl compared with using pure water (p < 0.05). The reduction in water permeability when salt solutions were filtered was most likely due to the polySPE brushes swelling inside the pores, strongly hindering convective liquid transport; this swelling increases with an increase in the salt concentration according to the "anti-polyelectrolyte" effect.[59,61−63] The permeance results at the different salt concentrations also support our assumption of LLP somewhat overestimating the pore size.

The surface morphologies of the pristine and microporous grafted membranes were analyzed using SEM. Compared with the external surface of the PES_pristine (Figures 5A and S5A), the pores of the modified membranes narrowed with the increasing SPE monomer concentration in the grafting solution (Figures 5B−D and S5B−D).

The membranes' cross-sectional morphologies were also analyzed by SEM. Figure 5E−H (and Figure S5E−H) shows that the sponge-like structure of the pristine membrane was preserved after grafting. Nevertheless, the interconnected networks of the brush-grafted membranes seem thicker with lower cross-sectional porosity than that of the pristine membrane. The cross-sectional and surface SEM images also

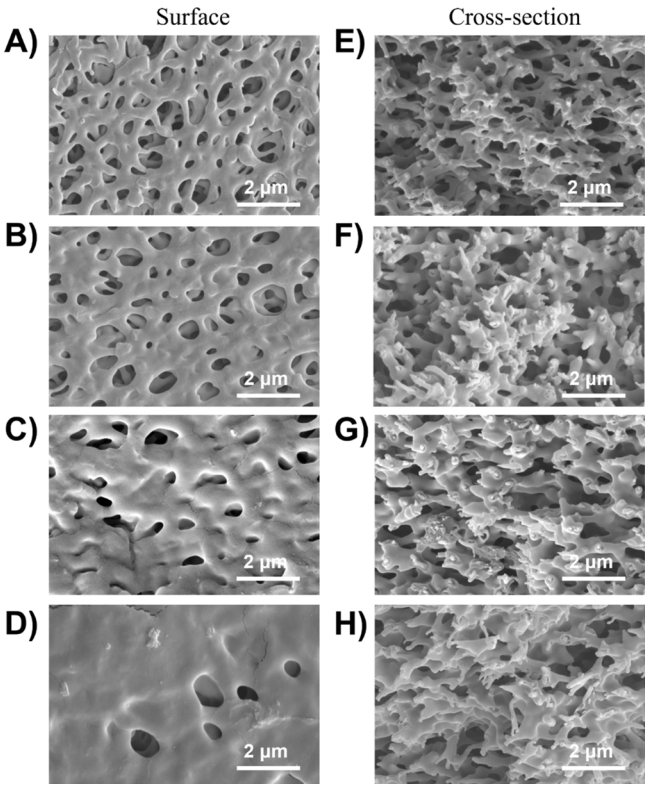

Figure 5. Surface and cross-sectional SEM images of PES_pristine (A,E), PES_0.1 (B,F), PES_0.2 (C,G), and PES_0.5 (D,H).

reveal that the grafting was not even throughout the cross-section: it occurred mostly near both sides of the membrane and less in the interior as was also reported by Bayat et al. for poly(diethylene glycol methyl ether methacrylate) (PDEGMA)-brush-filled anodic aluminum oxide membranes.[64] The cross-sectional structure renders the membrane asymmetric, but as the brush layer contains a high-water fraction,[65,66] the membrane is super-hydrophilic and the cross-section is highly porous, so the permeance of the brush-grafted membranes remained high.

3.2. Bacteriophage Removal. Figure 6 shows the average LRVs (eq 4) for T4 and NT1 bacteriophages by the membranes. The pristine membrane removed T4 much less well (0.4 LRV) than the microporous grafted membranes (2.4,

https://doi.org/10.1021/acsami.3c01495
ACS Appl. Mater. Interfaces 2023, 15, 18343−18353

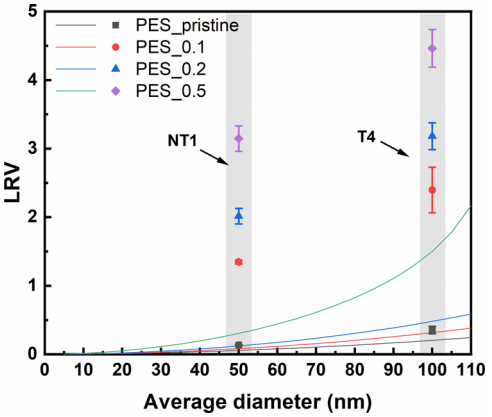

Figure 6. Experimental (symbols) and modeled (lines) LRVs for T4 and NT1 by PES_pristine and various grafted membranes. The experimental data are expressed as mean ± SD; $n = 3$.

3.2, and 4.5 LRV for PES_0.1, PES_0.2, and PES_0.5, respectively). The three grafted membranes removed NT1 much better (1.4, 2.0, and 3.1 LRV for PES_0.1, PES_0.2, and PES_0.5, respectively) than the unmodified membrane (0.1 LRV).

The theoretical LRVs were based solely on the hindrance transport model and calculated according to eqs 5−8. The removal of spherical particles with diameters ranging from 50 to 100 nm (Figure 6) indicates that the experimental and predicted removal rates of T4 and NT1 by PES_pristine matched. These LRVs indicate that size exclusion (screen filtration) was likely the main mechanism for bacteriophage removal by PES_pristine with negligible adsorption or entrapment. In contrast, although the model predicts LRV < 1 for T4 and NT1 by the modified membranes, the measured LRVs were much higher, indicating another removal mechanism.

As the mechanism of bacteriophage removal by the microporous brush-grafted membranes cannot be fully characterized by size exclusion, the observed LRVs could be due to increased repulsion forces between the bacteriophage and the brushes[36] or to the accumulation of bacteriophage in the grafted membranes through adsorption or physical entrapping. Accordingly, for the pristine and PES_0.1 membranes, we measured the amounts of bacteriophages in the different suspensions: the retentate, the backwash solution (i.e., reversibly deposited bacteriophage), and sonicated solution with the membrane submerged in the background solution (i.e., irreversibly deposited bacteriophage). Enhanced separation of bacteriophages was due to their accumulation within the membrane micropores (Table 2). We surmise that bacteriophages were accumulated even though not all of them were detached from the membrane. Notably, a smaller bacteriophage portion (~50%) was detected in the backwash of the microporous brush-grafted membrane, while a relatively higher portion was recovered from the membrane by sonication. It is likely that the microporous brush-grafted membrane entrapped a significant amount of bacteriophages, probably owing to changes in its cross-sectional morphology, increased porosity, and smaller pores, as evidenced by the LLP analysis and SEM images.

3.3. μ-XRF Synchrotron and NanoSIMS Analyses of the Effects of Brush Modification on the Deposition of Si-Coated Nanospheres on the Membranes. As bacteriophage removal by the brush-grafted membrane was measured to be much higher than estimated by size exclusion based on hindrance alone, another removal mechanism is clearly at play. The removal seems to have been improved by changes in the membrane's cross-sectional morphology, which resulted in the entrapment of the bacteriophages. To further study the influence of polySPE brushes on T4 and NT1 removal, synchrotron-based μ-XRF and NanoSIMS analyses provided high-resolution spatial determination of filtrated model nanoparticles through pristine and PES_0.5 membranes. The results revealed the spatial distribution of 100 nm model nanoparticles after similar filtration experiments of 10^7 nanoparticles/mL suspension in 10 mM NaCl through the membranes. Cross-sectional μ-XRF images (Figure S6) show the distribution of Au within the membrane. To compare the distributions across both membranes, Figure 7A,B presents the Au concentration (blue line), along with S intensity (red line), measured along a single line through each cross-section. For the pristine membrane (Figure 7A), the Au concentration begins to rise slightly before the S intensity and then decreases abruptly below the detection limit, indicating that the Au particles accumulate only at the membrane surface. This result suggests that these particles were either deposited on the membrane during filtration or passed through. For the PES_0.5 membrane (Figure 7B), no Au nanoparticles were deposited on the membrane surface, probably due to their exclusion by the surface-grafted brush. In addition, Au particles are visible inside the membrane, mainly in the upper third part of the membrane, suggesting that penetrated Au nanoparticles were entrapped in the membrane. The μ-XRF experiments were also conducted with an Au nanoparticles suspension in 8.5 mM NaCl and 0.5 mM $CaCl_2$ (Figures S7 and S8). Interestingly, while the Au profile in the presence of calcium for the pristine membrane was similar to the one recorded using NaCl, the Au intensity for the brush-grafted membrane was much higher inside the membrane, and Au particles were also detected on the membrane surface (but much less than for the pristine one). The higher intensity inside the brush-grafted membrane when calcium ions were present is unclear, and the effect of solution composition on membrane performance and particle retention, including bacteriophages, needs further investigation. Corroborating the μ-XRF analysis, the high-resolution NanoSIMS depth profile of Au ions provides evidence for the proposed mechanism of bacteriophage retention by the additional zwitterionic polymer brushes. The grafted membrane shows a significant initial increase in Au ion intensity

Table 2. Mass Balance of T4 Filtered, Backwashed, and Separated by Sonication for PES_pristine and PES_0.1: The Plaque-Forming Unit Was Used To Estimate Bacteriophage Counts[a]

	feed ×10^3 PFU	permeate ×10^3 PFU	reversible attachment ×10^3 PFU	irreversible attachment ×10^3 PFU	total ×10^3 PFU
pristine	2792 ± 264	980 ± 107	970 ± 100	299 ± 19	2249 ± 190
PES_0.1	2833 ± 314	11 ± 6	917 ± 103	1646 ± 235	2574 ± 330

[a]Total is the sum of permeate, reversible attachment, and irreversible attachment.

https://doi.org/10.1021/acsami.3c01495
ACS Appl. Mater. Interfaces 2023, 15, 18343−18353

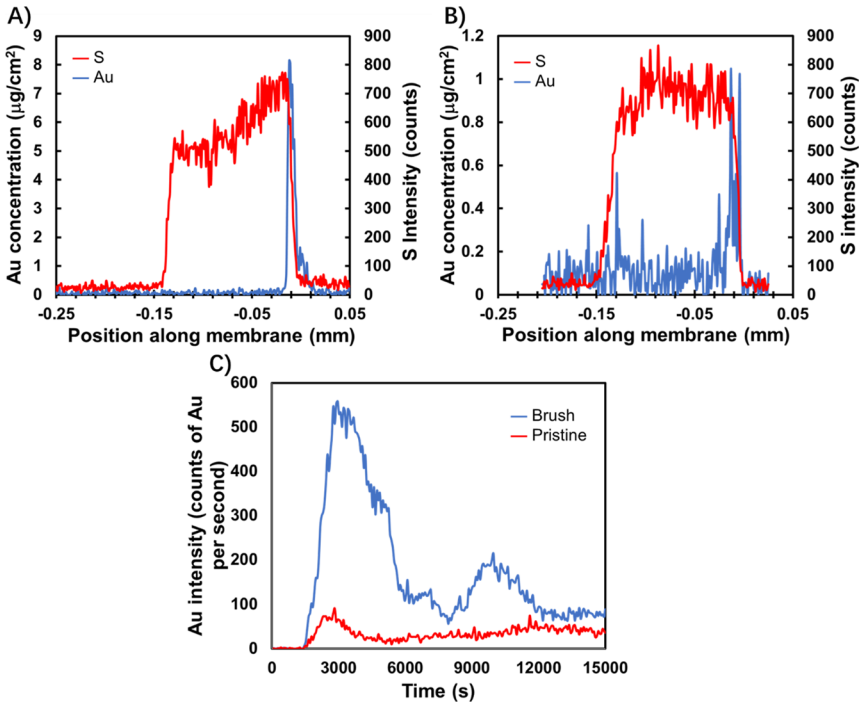

Figure 7. Locations of Si-coated Au spheres in the pristine and PES_0.5 membranes. (A,B) Profiles of the Au concentration (blue) and S intensity (red) along a single line of the membrane cross-section, imaged using μ-XRF. The x-axis is the position along the membrane cross-section, given in mm. Note the difference in Au concentration scale between the plots for each membrane (see images in Figure S6). (C) Depth profiles of $^{197}Au^-$ ions in PES and PES_0.5 filtered with Si-coated gold nanoparticles at 10^7 nanoparticles/mL in 10 mM NaCl solution. NanoSIMS parameters: scanning beam diameter of ~100 nm with a dwell time of 1000 μs/pixel and raster size of 20 μm from 256 × 256 pixels. Ions were extracted from a 50 × 50 nm area.

compared with the pristine membrane (Figure 7C), indicating a significantly higher entrapment of gold nanoparticles: the pristine PES membrane entrapped ~80% fewer Au particles than the PES_0.5 membrane. Brush−bacteriophage interactions might also contribute to bacteriophage removal. For example, recent molecular dynamics simulations have suggested that numerous stable direct contacts between nanoparticles and polymer brushes can occur, even when the brushes are extremely phobic to the nanoparticles.[67] Wang and Tarabara used quartz crystal microbalance with dissipation analysis to show the importance of interfacial interactions to the adsorption of viruses to surfaces.[24] Other theoretical models and simulations have provided insights into the penetration of biomolecules and colloids into zwitterionic polymer brush systems and the interactions between them.[68−70] Therefore, a fundamental investigation is needed on the partitioning and transport of viruses permeating into polymer brushes grafted to membranes and the nature of the interactions of the brushes with biomolecules or colloids.

4. CONCLUSIONS

Our study developed microporous polySPE brush-grafted MF membranes for removing viruses from water. ATR−FTIR and XPS analyses showed increasing degrees of brush grafting in membranes modified with an increasing concentration monomer and that the modification occurred through the membrane's microporous cross-section. Contact angle measurements showed that grafting made the membranes highly hydrophilic. SEM and LLP measurements revealed that the pore size and the pore-size distribution became narrower with grafting. These changes resulted in lower permeate water flux than shown by the pristine membrane; however, the grafted membranes were still in the MF range. The LRVs of the modified membranes significantly improved while the permeability was maintained in the MF range. Specifically, the removal rate increased from 0.5 LRV for the pristine membrane to 4.5 LRV for the microporous membrane grafted with polySPE brushes from 0.5 M monomer solution (PES_0.5). The contribution to bacteriophage removal by size exclusion and entrapment was analyzed by comparing results from hindrance modeling with the experimental data. A combined removal mechanism allowed the pores of the microporous brush-grafted membrane—which were larger than either of the tested bacteriophages—to achieve high removal rates. μ-XRF synchrotron and high-resolution nanoSIMS analyses showed that Si-coated gold nanospheres accumulated on the surface of the pristine membrane but not on the brush-coated membrane, and those nanospheres that penetrated the membranes were entrapped in the brush-grafted membrane but passed the pristine one. Although the entrapment of the particles (and likely bacteriophage) in the brushes plays a major role in bacteriophage removal, the interactions between bacteriophages and the brushes and even bacteriophages infiltration into the brush in different aqueous solutions should be further investigated to elucidate the complete mechanism. Overall, low-pressure polySPE microporous brush-grafted MF membranes provide a promising avenue for removing enteric viruses from water. Future studies should focus on the regeneration capacity of these microporous brush-grafted membranes.

https://doi.org/10.1021/acsami.3c01495
ACS Appl. Mater. Interfaces 2023, 15, 18343−18353

■ ASSOCIATED CONTENT

Supporting Information

The Supporting Information is available free of charge at https://pubs.acs.org/doi/10.1021/acsami.3c01495.

Schematic diagram of the two-step SI-ATRP method to graft zwitterionic polymer (polySPE) brushes inside the MF membrane pores; schematic diagram of the bench-scale dead-end filtration unit for testing bacteriophages removal; schematic illustration of log-phase *E. coli* culture; images of the positive and negative controls double agar layer plates; elemental composition obtained by high-resolution XPS of both sides of PES_pristine, PES_0.1, PES_0.2, and PES_0.5 membranes; surface and cross-sectional SEM images of the PES_pristine, PES_0.1, PES_0.2, and PES_0.5 membranes; cross-section μ-XRF images of the location of the Si-coated Au spheres in 10 mM NaCl solution at the pristine PES and PES_0.5 membranes; depth profiles of the Au concentration and sulfur intensity along a single line of the pristine PES and PES_0.5 membrane cross-section imaged using μ-XRF; and cross-section μ-XRF images of the location of the Si-coated Au spheres in 10 mM NaCl+$CaCl_2$ solution at the pristine PES and PES_0.5 membranes (PDF)

■ AUTHOR INFORMATION

Corresponding Authors

Moshe Herzberg − *Zuckerberg Institute for Water Research, The Jacob Blaustein Institutes for Desert Research of the Ben-Gurion University of the Negev, Midreshet 84990, Israel;* orcid.org/0000-0001-7065-0824; Email: herzberg@bgu.ac.il

Roy Bernstein − *Zuckerberg Institute for Water Research, The Jacob Blaustein Institutes for Desert Research of the Ben-Gurion University of the Negev, Midreshet 84990, Israel;* orcid.org/0000-0003-2275-181X; Email: royber@bgu.ac.il

Authors

Ji Qin − *Zuckerberg Institute for Water Research, The Jacob Blaustein Institutes for Desert Research of the Ben-Gurion University of the Negev, Midreshet 84990, Israel*

Eric Ziemann − *Zuckerberg Institute for Water Research, The Jacob Blaustein Institutes for Desert Research of the Ben-Gurion University of the Negev, Midreshet 84990, Israel*

Edo Bar-Zeev − *Zuckerberg Institute for Water Research, The Jacob Blaustein Institutes for Desert Research of the Ben-Gurion University of the Negev, Midreshet 84990, Israel;* orcid.org/0000-0001-6575-2068

Sharon E. Bone − *Stanford Synchrotron Radiation Lightsource, SLAC National Accelerator Laboratory, Menlo Park, California 94025, United States;* orcid.org/0000-0002-7521-9627

Yuanzhe Liang − *Civil and Environmental Engineering, Stanford University, Stanford, California 94305, United States*

Meagan S. Mauter − *Civil and Environmental Engineering, Stanford University, Stanford, California 94305, United States;* orcid.org/0000-0002-4932-890X

Complete contact information is available at: https://pubs.acs.org/10.1021/acsami.3c01495

Notes

The authors declare no competing financial interest.

■ ACKNOWLEDGMENTS

This work was supported by the Israel Science Foundation (ISF; grant no. 2554/21 to R.B.). Part of this work was performed at the Stanford Nano Shared Facilities (SNSF), supported by the National Science Foundation under Award ECCS-2026822. Y.L. and M.S.M. were supported by the National Alliance for Water Innovation (NAWI), funded by the U.S. Department of Energy, Energy Efficiency and Renewable Energy Office, Advanced Manufacturing Office under Funding Opportunity Announcement DE-FOA-0001905. Use of the SSRL, SLAC National Accelerator Laboratory, is supported by the U.S. Department of Energy, Office of Science, Office of Basic Energy Sciences, under Contract no. DE-AC02-76SF00515. E.Z. thanks the Kreitman School of Advanced Graduate Studies for support through the Hightech, Biotech, Chemotech, and Negev scholarship programs. Y.L. thanks the U.S. National Science Foundation (DMR-2023833) for financial support. M.H. thanks the Shimizu Visiting Professor Fellowship provided at Stanford University. The authors thank Dr. Natalya Froumin and Mrs. Roxana Golan from the Ilse Katz Institute for Nanoscale Science and Technology, BGU, for their help with XPS and SEM measurements and Dr. Christie Jilly-Rehak at the SNSF for technical assistance with NanoSIMS.

■ REFERENCES

(1) Domenico, B.; Alice, D. P. B.; Lorenza, L.; La Torre, G.; Cocchiara, R. A.; Sestili, C.; Del Cimmuto, A.; La Torre, G. The Impact of Environmental Alterations on Human Microbiota and Infectious Diseases. In *Environmental Alteration Leads to Human Disease: A Planetary Health Approach*; Springer: 2022; pp 209−227.

(2) Platts-Mills, J. A.; Babji, S.; Bodhidatta, L.; Gratz, J.; Haque, R.; Havt, A.; McCormick, B. J.; McGrath, M.; Olortegui, M. P.; Samie, A.; Shakoor, S.; Mondal, D.; Lima, I. F.; Hariraju, D.; Rayamajhi, B. B.; Qureshi, S.; Kabir, F.; Yori, P. P.; Mufamadi, B.; Amour, C.; Carreon, J. D.; Richard, S. A.; Lang, D.; Bessong, P.; Mduma, E.; Ahmed, T.; Lima, A. A.; Mason, C. J.; Zaidi, A. K.; Bhutta, Z. A.; Kosek, M.; Guerrant, R. L.; Gottlieb, M.; Miller, M.; Kang, G.; Houpt, E. R. Pathogen-Specific Burdens of Community Diarrhoea in Developing Countries: A Multisite Birth Cohort Study (MAL-ED). *Lancet Glob. Health* **2015**, *3*, e564−e575.

(3) U.S. Environmental Protection Agency. National Primary Drinking Water Regulations: Long Term 1 Enhanced Surface Water Treatment Rule (Final Rule). *Fed. Regist.* **2002**, *67*, 1811−1844.

(4) Masciopinto, C.; De Giglio, O.; Scrascia, M.; Fortunato, F.; La Rosa, G.; Suffredini, E.; Pazzani, C.; Prato, R.; Montagna, M. T. Human Health Risk Assessment for the Occurrence of Enteric Viruses in Drinking Water from Wells: Role of Flood Runoff Injections. *Sci. Total Environ.* **2019**, *666*, 559−571.

(5) Gude, V. G. Desalination and Water Reuse to Address Global Water Scarcity. *Rev. Environ. Sci. Bio/Technol.* **2017**, *16*, 591−609.

(6) Graham, K. E.; Anderson, C. E.; Boehm, A. B. Viral Pathogens in Urban Stormwater Runoff: Occurrence and Removal via Vegetated Biochar-Amended Biofilters. *Water Res.* **2021**, *207*, No. 117829.

(7) Kotwal, G.; Cannon, J. L. Environmental Persistence and Transfer of Enteric Viruses. *Curr. Opin. Virol.* **2014**, *4*, 37−43.

(8) Kim, S. J.; Si, J.; Lee, J. E.; Ko, G. Temperature and Humidity Influences on Inactivation Kinetics of Enteric Viruses on Surfaces. *Environ. Sci. Technol.* **2012**, *46*, 13303−13310.

(9) Shirasaki, N.; Matsushita, T.; Matsui, Y.; Oshiba, A.; Ohno, K. Estimation of Norovirus Removal Performance in a Coagulation−Rapid Sand Filtration Process by Using Recombinant Norovirus VLPs. *Water Res.* **2010**, *44*, 1307−1316.

(10) Kitajima, M.; Iker, B. C.; Pepper, I. L.; Gerba, C. P. Relative Abundance and Treatment Reduction of Viruses During Wastewater Treatment Processes—Identification of Potential Viral Indicators. *Sci. Total Environ.* **2014**, *488*, 290−296.
(11) Elliott, M.; DiGiano, F.; Sobsey, M. Virus Attenuation by Microbial Mechanisms During the Idle Time of a Household Slow Sand Filter. *Water Res.* **2011**, *45*, 4092−4102.
(12) Li, X.-F.; Mitch, W. A. Drinking Water Disinfection Byproducts (DBPs) and Human Health Effects: Multidisciplinary Challenges and Opportunities. *Environ. Sci. Technol.* **2018**, *52*, 1681−1689.
(13) Li, D.; Gu, A. Z.; He, M.; Shi, H.-C.; Yang, W. UV Inactivation and Resistance of Rotavirus Evaluated by Integrated Cell Culture and Real-Time RT-PCR Assay. *Water Res.* **2009**, *43*, 3261−3269.
(14) Salgot, M.; Folch, M.; Huertas, E.; Tapias, J.; Avellaneda, D.; Girós, G.; Brissaud, F.; Vergés, C.; Molina, J.; Pigem, J. Comparison of Different Advanced Disinfection Systems for Wastewater Reclamation. Water Supply 2002, *2* (3), 213−218, DOI: 10.2166/ws.2002.0105.
(15) Goswami, K. P.; Pugazhenthi, G. Credibility of Polymeric and Ceramic Membrane Filtration in the Removal of Bacteria and Virus from Water: A Review. *J. Environ. Manage.* **2020**, *268*, No. 110583.
(16) Chen, C.; Guo, L.; Yang, Y.; Oguma, K.; Hou, L. A.; Hou, L.-A. Comparative Effectiveness of Membrane Technologies and Disinfection Methods for Virus Elimination in Water: A Review. *Sci. Total Environ.* **2021**, *801*, No. 149678.
(17) Ibrahim, Y.; Ouda, M.; Kadadou, D.; Banat, F.; Naddeo, V.; Alsafar, H.; Yousef, A. F.; Barceló, D.; Hasan, S. W. Detection and Removal of Waterborne Enteric Viruses from Wastewater: A Comprehensive Review. *J. Environ. Chem. Eng.* **2021**, *9*, No. 105613.
(18) Trilisky, E. I.; Lenhoff, A. M. Flow-Dependent Entrapment of Large Bioparticles in Porous Process Media. *Biotechnol. Bioeng.* **2009**, *104*, 127−133.
(19) Schäfer, A.; Fane, A. G.; Waite, T. Cost Factors and Chemical Pretreatment Effects in the Membrane Filtration of Waters Containing Natural Organic Matter. *Water Res.* **2001**, *35*, 1509−1517.
(20) Sinclair, T.; Robles, D.; Raza, B.; Van den Hengel, S.; Rutjes, S.; de Roda Husman, A.; de Grooth, J.; de Vos, W.; Roesink, H. Virus Reduction through Microfiltration Membranes Modified with a Cationic Polymer for Drinking Water Applications. *Colloids Surf., A* **2018**, *551*, 33−41.
(21) Nasir, A. M.; Adam, M. R.; Kamal, S. N. E. A. M.; Jaafar, J.; Othman, M. H. D.; Ismail, A. F.; Aziz, F.; Yusof, N.; Bilad, M. R.; Mohamud, R. A Review of the Potential of Conventional and Advanced Membrane Technology in the Removal of Pathogens from Wastewater. *Sep. Purif. Technol.* **2022**, *286*, No. 120454.
(22) Dang, H. T.; Tarabara, V. V. Virus Deposition onto Polyelectrolyte-Coated Surfaces: A Study with Bacteriophage MS2. *J. Colloid Interface Sci.* **2019**, *540*, 155−166.
(23) Farrah, S. R. Chemical Factors Influencing Adsorption of Bacteriophage MS2 to Membrane Filters. *Appl. Environ. Microbiol.* **1982**, *43*, 659−663.
(24) Wang, X.; Tarabara, V. V. Virus Adhesion to Archetypal Fomites: A Study with Human Adenovirus and Human Respiratory Syncytial Virus. *Chem. Eng. J.* **2022**, *429*, No. 132085.
(25) Shirasaki, N.; Matsushita, T.; Matsui, Y.; Murai, K. Assessment of the Efficacy of Membrane Filtration Processes to Remove Human Enteric Viruses and the Suitability of Bacteriophages and a Plant Virus as Surrogates for Those Viruses. *Water Res.* **2017**, *115*, 29−39.
(26) Langlet, J.; Gaboriaud, F.; Duval, J. F.; Gantzer, C. Aggregation and Surface Properties of F-Specific Rna Phages: Implication for Membrane Filtration Processes. *Water Res.* **2008**, *42*, 2769−2777.
(27) Langlet, J.; Ogorzaly, L.; Schrotter, J.-C.; Machinal, C.; Gaboriaud, F.; Duval, J. F.; Gantzer, C. Efficiency of MS2 Phage and Qβ Phage Removal by Membrane Filtration in Water Treatment: Applicability of Real-Time RT-PCR Method. *J. Membr. Sci.* **2009**, *326*, 111−116.
(28) Van Voorthuizen, E.; Ashbolt, N.; Schäfer, A. Role of Hydrophobic and Electrostatic Interactions for Initial Enteric Virus Retention by MF Membranes. *J. Membr. Sci.* **2001**, *194*, 69−79.
(29) Brickey, K. P.; Zydney, A. L.; Gomez, E. D. Fib-Sem Tomography Reveals the Nanoscale 3d Morphology of Virus Removal Filters. *J. Membr. Sci.* **2021**, *640*, No. 119766.
(30) Sinclair, T.; Patil, A.; Raza, B.; Reurink, D.; Van den Hengel, S.; Rutjes, S.; de Roda Husman, A.; Roesink, H.; De Vos, W. Cationically Modified Membranes Using Covalent Layer-by-Layer Assembly for Antiviral Applications in Drinking Water. *J. Membr. Sci.* **2019**, *570*, 494−503.
(31) Wang, R.; Guan, S.; Sato, A.; Wang, X.; Wang, Z.; Yang, R.; Hsiao, B. S.; Chu, B. Nanofibrous Microfiltration Membranes Capable of Removing Bacteria, Viruses and Heavy Metal Ions. *J. Membr. Sci.* **2013**, *446*, 376−382.
(32) Hadidi, M.; Zydney, A. L. Fouling Behavior of Zwitterionic Membranes: Impact of Electrostatic and Hydrophobic Interactions. *J. Membr. Sci.* **2014**, *452*, 97−103.
(33) Zhang, W.; Yang, Z.; Kaufman, Y.; Bernstein, R. Surface and Anti-Fouling Properties of a Polyampholyte Hydrogel Grafted onto a Polyethersulfone Membrane. *J. Colloid Interface Sci.* **2018**, *517*, 155−165.
(34) Rahimi, A.; Mahdavi, H. Zwitterionic-Functionalized GO/PVDF Nanocomposite Membranes with Improved Anti-Fouling Properties. *J. Water Process. Eng.* **2019**, *32*, No. 100960.
(35) Chen, P.; Lang, J.; Zhou, Y.; Khlyustova, A.; Zhang, Z.; Ma, X.; Liu, S.; Cheng, Y.; Yang, R. An Imidazolium-Based Zwitterionic Polymer for Antiviral and Antibacterial Dual Functional Coatings. *Sci. Adv.* **2022**, *8*, No. eabl8812.
(36) Lu, R.; Zhang, C.; Piatkovsky, M.; Ulbricht, M.; Herzberg, M.; Nguyen, T. H. Improvement of Virus Removal Using Ultrafiltration Membranes Modified with Grafted Zwitterionic Polymer Hydrogels. *Water Res.* **2017**, *116*, 86−94.
(37) Getachew, B. A.; Guo, W.; Zhong, M.; Kim, J.-H. Asymmetric Hydrogel-Composite Membranes with Improved Water Permeability and Self-Healing Property. *J. Membr. Sci.* **2019**, *578*, 196−202.
(38) Al-kharabsheh, S.; Bernstein, R. Thin-Film Composite Polyionic Liquid Gel Membranes and Their Potential for Nanofiltration in Organic Solvents. *Adv. Mater. Interfaces* **2018**, *5*, No. 1800823.
(39) Ziemann, E.; Coves, T.; Levin, O.; Bernstein, R. Zwitterion Polymer Brushes on Porous Membranes: Characterization, Tribology, Performance, and the Effect of Electrolyte Anions. *ACS Appl. Polym. Mater.* **2020**, *2*, 4613−4625.
(40) Pieracci, J.; Crivello, J. V.; Belfort, G. Photochemical Modification of 10 kDa Polyethersulfone Ultrafiltration Membranes for Reduction of Biofouling. *J. Membr. Sci.* **1999**, *156*, 223−240.
(41) Pieracci, J.; Wood, D. W.; Crivello, J. V.; Belfort, G. UV-Assisted Graft Polymerization of N-Vinyl-2-Pyrrolidinone onto Poly (Ether Sulfone) Ultrafiltration Membranes: Comparison of Dip Versus Immersion Modification Techniques. *Chem. Mater.* **2000**, *12*, 2123−2133.
(42) Adams, M. H. Bacteriophages. In *Bacteriophages*; 1959.
(43) Webb, S. In The Microanalysis Toolkit: X-Ray Fluorescence Image Processing Software; AIP Conference Proceedings; American Institute of Physics; 2011; pp 196−199.
(44) Bungay, P. M.; Brenner, H. The Motion of a Closely-Fitting Sphere in a Fluid-Filled Tube. *Int. J. Multiphase Flow* **1973**, *1*, 25−56.
(45) Zhu, Y.; Chen, R.; Li, Y.-Y.; Sano, D. Virus Removal by Membrane Bioreactors: A Review of Mechanism Investigation and Modeling Efforts. *Water Res.* **2021**, *188*, No. 116522.
(46) Zachary, A. Isolation of Bacteriophages of the Marine Bacterium Beneckea Natriegens from Coastal Salt Marshes. *Appl. Microbiol.* **1974**, *27*, 980−982.
(47) Rao, V. B.; Black, L. W. Structure and Assembly of Bacteriophage T4 Head. *Virol. J.* **2010**, *7*, 356.
(48) Zeman, L.; Wales, M. Polymer Solute Rejection by Ultrafiltration Membranes. In *Synthetic Membranes: Volume II*; ACS, 1981, 411 −434.
(49) Eihadidy, A. M.; Peldszus, S.; Van Dyke, M. I. An Evaluation of Virus Removal Mechanisms by Ultrafiltration Membranes Using MS2 and Φx174 Bacteriophage. *Sep. Purif. Technol.* **2013**, *120*, 215−223.

(50) Giglia, S.; Bohonak, D.; Greenhalgh, P.; Leahy, A. Measurement of Pore Size Distribution and Prediction of Membrane Filter Virus Retention Using Liquid−Liquid Porometry. *J. Membr. Sci.* **2015**, *476*, 399−409.
(51) Zydney, A. L.; Aimar, P.; Meireles, M.; Pimbley, J. M.; Belfort, G. Use of the Log-Normal Probability Density Function to Analyze Membrane Pore Size Distributions: Functional Forms and Discrepancies. *J. Membr. Sci.* **1994**, *91*, 293−298.
(52) Hu, X.; Lin, X.; Zhao, H.; Chen, Z.; Yang, J.; Li, F.; Liu, C.; Tian, F. Surface Functionalization of Polyethersulfone Membrane with Quaternary Ammonium Salts for Contact-Active Antibacterial and Anti-Biofouling Properties. *Materials* **2016**, *9*, 376.
(53) Yang, F.; Huang, J.; Deng, L.; Zhang, Y.; Dang, G.; Shao, L. Hydrophilic Modification of Poly (Aryl Sulfone) Membrane Materials toward Highly-Efficient Environmental Remediation. *Front. Chem. Sci. Eng.* **2022**, *16*, 614−633.
(54) Zhong, P. S.; Widjojo, N.; Chung, T.-S.; Weber, M.; Maletzko, C. Positively Charged Nanofiltration (NF) Membranes Via UV Grafting on Sulfonated Polyphenylenesulfone (sPPSU) for Effective Removal of Textile Dyes from Wastewater. *J. Membr. Sci.* **2012**, *417*, 52−60.
(55) Singh, N.; Husson, S. M.; Zdyrko, B.; Luzinov, I. Surface Modification of Microporous Pvdf Membranes by ATRP. *J. Membr. Sci.* **2005**, *262*, 81−90.
(56) Rusen, E.; Şomoghi, R.; Busuioc, C.; Diacon, A. Hydrophilic Modification of Polyvinyl Chloride with Polyacrylic Acid Using ATRP. *RSC Adv.* **2020**, *10*, 35692−35700.
(57) Lounder, S. J.; Asatekin, A. Zwitterionic Ion-Selective Membranes with Tunable Subnanometer Pores and Excellent Fouling Resistance. *Chem. Mater.* **2021**, *33*, 4408−4416.
(58) Barth, M.; Wiese, M.; Ogieglo, W.; Go, D.; Kuehne, A. J.; Wessling, M. Monolayer Microgel Composite Membranes with Tunable Permeability. *J. Membr. Sci.* **2018**, *555*, 473−482.
(59) Adrus, N.; Ulbricht, M. Novel Hydrogel Pore-Filled Composite Membranes with Tunable and Temperature-Responsive Size-Selectivity. *J. Mater. Chem.* **2012**, *22*, 3088−3098.
(60) Tufani, A.; Ince, G. O. Smart Membranes with Ph-Responsive Control of Macromolecule Permeability. *J. Membr. Sci.* **2017**, *537*, 255−262.
(61) Wang, T.; Wang, X.; Long, Y.; Liu, G.; Zhang, G. Ion-Specific Conformational Behavior of Polyzwitterionic Brushes: Exploiting It for Protein Adsorption/Desorption Control. *Langmuir* **2013**, *29*, 6588−6596.
(62) Das, S.; Banik, M.; Chen, G.; Sinha, S.; Mukherjee, R. Polyelectrolyte Brushes: Theory, Modelling, Synthesis and Applications. *Soft Matter* **2015**, *11*, 8550−8583.
(63) Mary, P.; Bendejacq, D. D.; Labeau, M.-P.; Dupuis, P. Reconciling Low-and High-Salt Solution Behavior of Sulfobetaine Polyzwitterions. *J. Phys. Chem. B* **2007**, *111*, 7767−7777.
(64) Bayat, H.; Raoufi, M.; Zamrik, I.; Schönherr, H. Poly (Diethylene Glycol Methylether Methacrylate) Brush-Functionalized Anodic Alumina Nanopores: Curvature-Dependent Polymerization Kinetics and Nanopore Filling. *Langmuir* **2020**, *36*, 2663−2672.
(65) Yang, Z.; Zhang, S.; Tarabara, V. V.; Bruening, M. L. Aqueous Swelling of Zwitterionic Poly (Sulfobetaine Methacrylate) Brushes in the Presence of Ionic Surfactants. *Macromolecules* **2018**, *51*, 1161−1171.
(66) Emilsson, G.; Xiong, K.; Sakiyama, Y.; Malekian, B.; Gagnér, V. A.; Schoch, R. L.; Lim, R. Y.; Dahlin, A. B. Polymer Brushes in Solid-State Nanopores Form an Impenetrable Entropic Barrier for Proteins. *Nanoscale* **2018**, *10*, 4663−4669.
(67) Etha, S. A.; Pial, T. H.; Das, S. Extensive Stable Physical Contacts between a Nanoparticle and a Highly Repulsive Polymeric Layer. *J. Phys. Chem. B* **2022**, *126*, 5715−5725.
(68) Milchev, A.; Dimitrov, D.; Binder, K. Excess Free Energy of Nanoparticles in a Polymer Brush. *Polymer* **2008**, *49*, 3611−3618.
(69) Oren, R.; Liang, Z.; Barnard, J. S.; Warren, S. C.; Wiesner, U.; Huck, W. T. Organization of Nanoparticles in Polymer Brushes. *J. Am. Chem. Soc.* **2009**, *131*, 1670−1671.
(70) Tagliazucchi, M.; Huang, K.; Szleifer, I. Routes for Nanoparticle Translocation through Polymer-Brush-Modified Nanopores. *J. Phys.: Condens. Matter* **2018**, *30*, 274006.

https://doi.org/10.1021/acsami.3c01495
ACS Appl. Mater. Interfaces 2023, 15, 18343−18353